MICHIGAN STATE UNIVERSITY

CYCLOTRON LABORATORY

LIGHT PARTICLE EMISSION IN HEAVY-ION COLLISIONS

DAVID K. SCOTT

Talk presented at the 3rd ADRIATIC EUROPHYSICS CONFERENCE
ON THE DYNAMICS OF HEAVY ION COLLISIONS,
HVAR, JUGOSLAVIA, 1981.

JULY 1981

MSUCL-355

MSUCL-355
July 1981

LIGHT PARTICLE EMISSION IN HEAVY-ION COLLISIONS

David K. SCOTT

National Superconducting Laboratory
and
Departments of Physics and Chemistry
Michigan State University
East Lansing, Michigan 48824, USA

Abstract: Some aspects of light particle emission in heavy-ion collisions are discussed over a broad energy region from about 10 MeV/nucleon up to relativistic energies of 1 GeV/nucleon. The appearance of high energy components above the equilibrium evaporation region of the spectra is shown to be a general feature. At all energies the contributions to this tail are likely to range from single nucleon-nucleon up to multiple nucleon collisions. Various theories have been developed to describe the processes, ranging from the microscopic models of DWBA, master equation, cascade and TDHF to the macroscopic hydrodynamic, participant-spectator and hot-spot reaction mechanisms. A common feature of the macroscopic models is the formation of a localised participant zone in thermal equilibrium at high temperature. Systematics on the existence of this zone are presented over a wide range of energies, but other explanations in terms of simpler direct processes cannot be ruled out at this stage. The relation to short mean free paths and the contrast with low temperature mean field theories which ignore nucleon-nucleon collisions are mentioned. Various approaches to determining the size of the localised zones are presented, such as the geometry of the participant and hot-spot models, the formation of composite light particles by coalescence or by chemical equilibrium, and experiments on two particle intensity interferometry. Studies of the light particles, in particular the deuteron-proton ratio, to determine the entropy of the hot zone are also described. Although the observed excess at high energies is presently attributed to the influence of additional degrees of freedom, eg. from phase transitions, a note of caution is raised by similar studies at lower energies. It is possible that deuterons are also created by simpler mechanisms, eg. by the snowball and surface pick-up effects. Finally it is shown that the multiplicity of light particles, by probing the disintegration of the hot zone, can also give information on the equation of state of nuclear matter.

1. Introduction

The emission of light particles is now a frequently studied aspect of nuclear collisions, not only because light particles are often the most probable outcome of the reaction but also because they are a copious source of information about the mechanisms. In concert with the huge amount of experimental data amassed at incident energies from a few MeV/nucleon to relativisitic energies of several GeV/nucleon, there exists a plethora of theoretical interpretations, ranging from microscopic approaches of TDHF, pre-equilibrium and cascade models to the more macroscopic theories of nuclear hydrodynamics, hot spots, and participant-spectator models. In addition to supplementing the knowledge derived from light-ion reactions on the evolution of nuclear systems towards global or partial equilibrium, the light particles produced in heavy-ion collisions may also serve as harbingers of the conditions prevailing in the hot, dense matter presumed to be created at relativistic energies. In this paper we discuss recent results on light particle emission, emphasizing the insight to be gained by systematic studies over a wide energy region.

2. General features of light particle emission

At low incident energies of a few MeV/nucleon, heavy-ion reactions generally lead to the formation of a compound nucleus or to a rotating dinuclear system. In both cases the initial collective energy of relative motion is dissipated on a fast time scale of a few times 10^{-22} sec. The emitted light particles then reflect the equilibrium temperature of the compound nucleus or the dinuclear system. A good example[1]) is shown in fig. 1(a)† for neutron emission from $^{56}Fe + ^{165}Ho$ at 8.5 MeV/nucleon, i.e. at about 4 MeV/nucleon above the barrier in the center-of-mass system. The spectra are shown in the rest frames of the light (open circles) and heavy (filled squares) fragments, and are averaged over a wide range of energy losses. It is clear that the two fragments have acquired the same temperature as required if complete statistical equilibrium is achieved. The solid curves correspond to the function $\sqrt{E}\exp(-E/T)$ with T=2 MeV, which is close to the equilibrium temperature of the system.

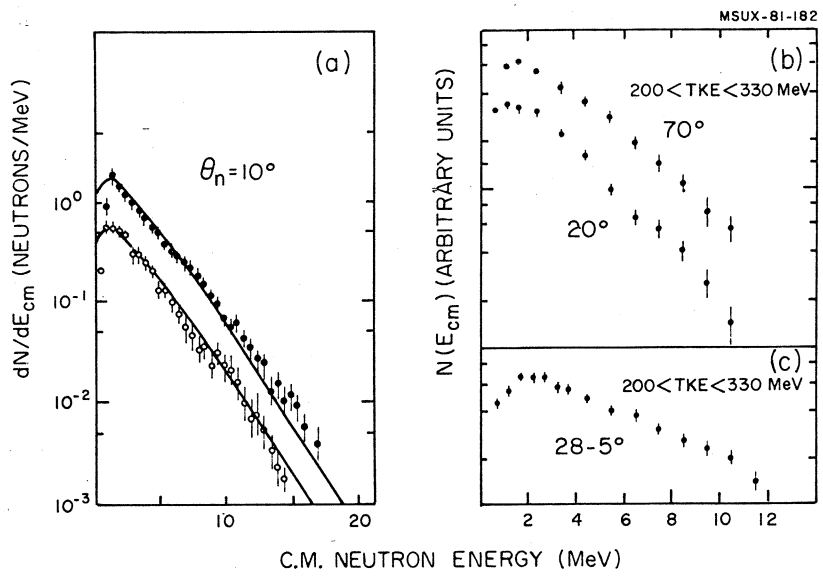

FIG. 1. Neutron spectra from deep-inelastic reactions: (a) $^{56}Fe + ^{165}Ho$ at 8.5 MeV/nucleon in rest frames of light (open circles) and heavy fragment (filled circles); (b) $^{86}Kr + ^{166}Er$ at 11.9 MeV/nucleon from light (20°) and heavy fragment (70°); (c) as in (b) from light fragment at 28.5°.

Now compare the system ^{86}Kr on ^{166}Er at the higher energy of 11.9 MeV/nucleon in (b) and (c), corresponding to 7.5 MeV/nucleon above the barrier in c.m. system. In (b) the spectra of neutrons associated with[2]) the light (20°) and heavy fragments (70°) have similar slopes, showing that equilibrium was also reached for the deep-inelastic events (TKE, the total energy loss, between 200 to 330 MeV) but the neutron spectrum in (c), associated with emission from the heavy fragment at a more forward angle of 28.5°, has a quite different slope, and cannot be accounted for by assuming isotropic evaporation. A non-equilibrium component is present. The results of many experiments show that it sets in at incident energies above 5 MeV/nucleon above the barrier.[1])

At incident energies of 20 MeV/nucleon, the pre-equilibrium component becomes a dominant feature of the spectrum. As shown in fig. 2 for $^{16}O + ^{238}U$ at 310 MeV, two components are clearly visible in the spectra.[3,4]) An equilibrium, evaporation component (extrapolated by the dashed line) is dominant at emitted neutron energies

below 10 MeV and corresponds to a temperature of about 2.7 MeV; using the Fermi gas relation,

$$E^* = \frac{A}{8} T^2 \quad ,$$

we expect an equilibrium temperature for A = 254 and E ≈ 215 MeV (the available energy above the barrier) of 2.6 MeV. At high energies, above 20 MeV, the spectra develop a pre-equilibrium tail, many orders of magnitude above the equilibrium component.

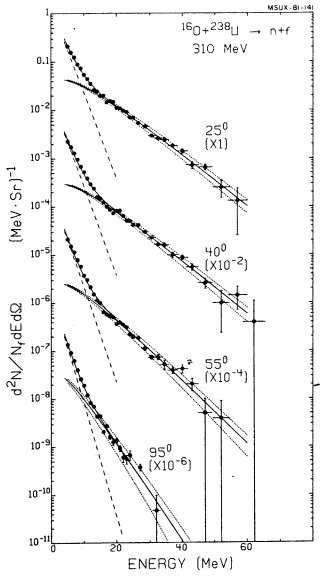

FIG. 2. Neutron spectra in coincidence with fission fragments from ^{16}O + ^{238}U at 310 MeV.

Some appreciation of the rapid increase in the cross section for pre-equilibrium emission is shown by the plot in fig. 3 of the multiplicity of emitted charged particles[5] (protons to alphas) as a function of incident energy per nucleon above the barrier. (We shall see later that the spectra for charged particles exhibit features very similar to those of neutrons). In this plot the contributions from compound nuclear processes are excluded. The multiplicity of charged particles, defined as the ratio of the integrated charged particle cross section divided by the reaction cross section, $\pi r_0^2 (A_1^{1/3} + A_2^{1/3})$, increases rapidly between 5 and 15 MeV/nucleon for the systems ^{16}O + Au and Al. At much higher energies of 250 MeV/nucleon to 1 GeV/nucleon, multiplicities have also been determined and are shown for the comparable system ^{20}Ne + U. Although an exact comparison with the lower energies is not possible on account of different instrumental cut-offs, the data already raise interesting questions, both on the multiplicity increase and ultimate magnitude. We shall return to these points later in this paper.

For the present we note that a rapid increase in cross section for pre-equilibrium particle emission is already predicted in calculations with the Boltzmann master equation.[6] This approach has only recently been applied to heavy-ion reactions, although it has long been a successful prescription for pre-equilibrium emission in light-ion reactions. The underlying reasons for the small pre-equilibrium contribution from heavy-ion reactions in the deep-inelastic regime is illustrated[7] in fig. 4. At energies of a few MeV/nucleon, the relative velocity of

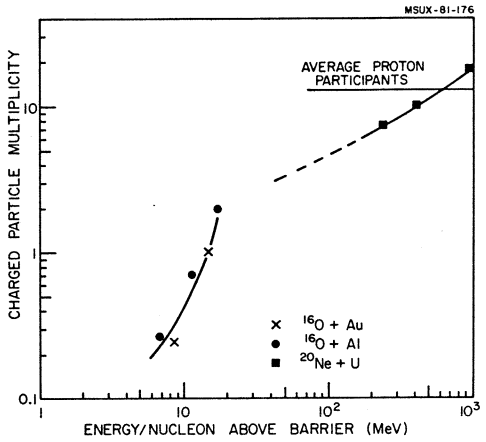

FIG. 3. Charged particle multiplicities as a function of incident energy/ nucleon above the barrier.

the nuclei is small and the energy loss at each step of the collision, Δ, is very small, $\approx \hbar\nu/R \approx 1$ MeV. Consequently many hundreds of steps are necessary to dissipate the initial energy. It is unlikely that the excited particle-hole states can decay by pre-equilibrium emission. The situation is quite different for a light-ion reaction at 100 MeV, where the energy loss per step is typically 20 MeV, the number

MSUX-81-177

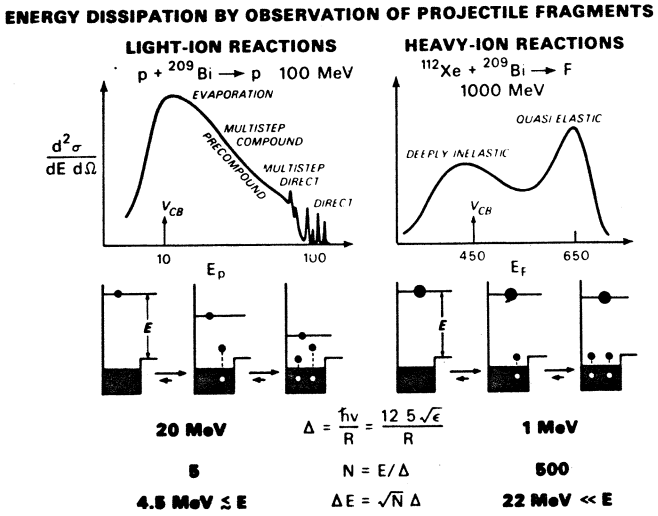

FIG. 4. Schematic representation of energy loss by particle-hole excitation in light and heavy-ion induced reactions. The typical energy loss per step Δ, number of steps to dissipate the entire energy N, and the fluctuations ΔE are indicated.

of steps $N = E/\Delta$ is small, and furthermore the fluctuations $\delta E = \sqrt{N}\Delta$ are large and comparable to E. The probability of decay by fast particle emission at each step is also large. Clearly heavy-ion reactions at higher energies of 20 MeV/nucleon and upwards should also exhibit pronounced pre-equilibrium features.

The number of collisions contributing to the high energy tails of light particle spectra plays a central role in high energy, relativistic heavy-ion collisions. Only if there are many collisions can the ideas of equilibrium and hydrodynamics apply (at least in the usual sense). It is therefore interesting to compare hadron and heavy-ion induced pre-equilibrium emission at different energies. A comparison of neutron emission in three reactions is made in fig. 5, for the $^{16}O + ^{238}U$ reaction[4]) at 20 MeV/nucleon discussed previously, the $^{20}Ne + U$ reaction at 337 MeV/nucleon[8]) and the reaction[9]) of protons on tantalum at 30 MeV. Superficially all three reactions behave in a similar fashion, containing a low energy equilibrium component and a high energy tail, the origin of which is likely to be similar in all three reactions. In the hadron case, it is known that the tail is due mainly to one or two nucleon-nucleon collisions,[10]) whereas the equilibrated component is the result of more than 3 collisions. For heavy-ion collisions at high-energy, cascade calculations show[11]) that there are contributions from one to several nucleon-nucleon collisions, and that the tail contains a substantial contribution (≈30% for Ne + U) from processes in which local equilibrium is indeed reached.[12]) No simple division into direct and thermal components is possible in general; rather there is a continuously rising departure from equilibrium as the number of collisions decreases. For heavy-ion collisions at lower energies of 20 MeV/nucleon, there is as yet no detailed knowledge of the relative contributions of direct and thermal components, but both are likely to be in force.

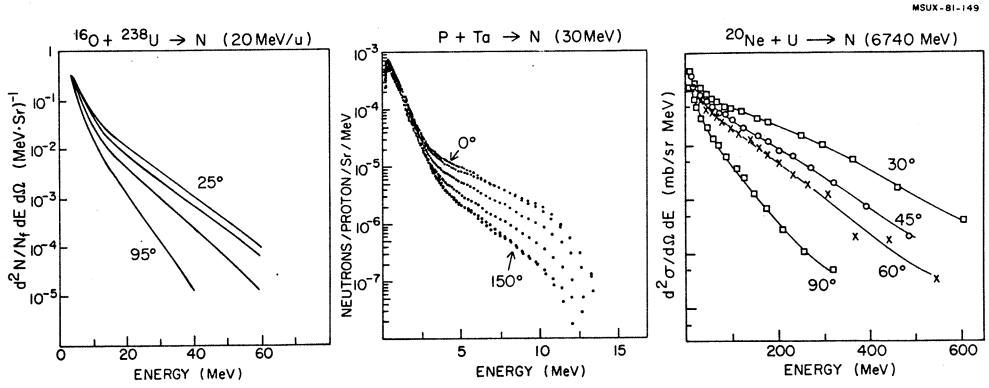

FIG. 5. Comparison of pre-equilibrium neutron spectra for $^{16}O + ^{238}U$ at 20 MeV/nucleon, p + Ta at 30 MeV and $^{20}Ne + U$ at 337 MeV/nucleon.

Theoretical methods applicable over the whole range of energies and colliding nuclei are available,[13]) and will no doubt answer these questions in due course. In the meanwhile we must be content with a variety of phenomenological approaches. It is possible, for example, that fluctuations in the energy division between the nuclei in deep-inelastic scattering causes deviations from the slope associated with the equilibrated division in proportion to the masses.[14]) Also Fermi jets or PEPS (promptly emitted particles) may contribute;[15]) through this mechanism high energy particles are emitted when the incident nucleon velocity couples with the intrinsic Fermi motion as the particle passes freely through the neck opened up between the colliding nuclei. This mechanism therefore results from no nuclear collisions, and has its origin in the long mean free path attributed to nucleons in nuclei.

These fast light particles can be seen in the density contours of a TDHF calculation for $^{12}C + Au$ at 30 MeV/nucleon in fig. 6 for both peripheral (b=6 fm)

and central (b=1 fm) collisions.[16]) The outermost contour line has density 0.14 x 2^{-NC+1} nucleons/fm^3 and successive inner contours have densities lower by a factor of 2. In the central collision, a high velocity jet of dilute matter (free nucleons) escapes, whereas for the peripheral case a large part of the projectile is captured and a few nucleons escape. It seems unlikely that this process is the main contributor at 20 MeV/nucleon, in view of the similarity to other reactions where one or several collisions is known to take place. The distinction is important, since the contribution from nucleon-nucleon collisions determines the deviation from mean field theories, the relevance of hydrodynamical models in addition to the mean free path of nucleons in nuclear matter. Such considerations have led to

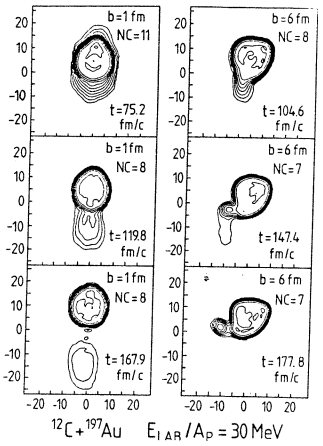

FIg. 6. TDHF calcualtions for ^{12}C + ^{197}Au at 30 MeV/nucleon, showing density contours for central (b=1 fm) and peripheral (b=6 fm) collisions.

models in which the high energy tails are produced from local high temperatures created in a hot zone.[17-20]) This concept may provide a connecting link to the participant or fireball zone in high-energy nuclear collisions, in which local equilibrium is reached. At the other extreme there are the simple processes of projectile fragmentation and delayed fragmentation[21, 22]) which can yield high energy light particles without invoking the above exotic considerations. In the region of 20 MeV/nucleon we also know that incomplete fusion[23]) and incomplete deep-inelastic scattering[24]) are important. Here a light fragment escapes promptly on collision and the remaining part of the projectile fuses or interacts with the target. By invoking the balance of nuclear, Coulomb and centrifugal forces to determine a critical angular momentum ℓ_c

$$4\pi\gamma\frac{R_1R_2}{R_1+R_2} = \frac{Z_1Z_2e^2}{(R_1+R_2)^2} + \frac{\ell_c(\ell_c+1)\hbar^2}{\mu(R_1+R_2)^3}$$

one finds that at 20 MeV/nucleon, the critical angular momentum for all fragments of the projectile is surpassed. It is natural therefore to expect an onset of fast light particle emission (recall figs. 3, and 5).

A graphic illustration of the onset of high multiplicity light particle emission, and also of the need for exclusive measurements, is given in the streamer chamber and emulsion photographs of fig. 7. The bottom left hand frame shows the outcome of a typical, low energy heavy-ion reaction; a carbon beam of 25 MeV/nucleon is incident from the left and collides with ^{20}Ne, leading to three particles in the final state.[25]) At the opposite extreme is the collision of ^{40}Ar at

1800 MeV/nucleon in an emulsion,[26]) in which both nuclei are completely shattered. But there are intimations of these explosive events already at 25 MeV/nucleon as illustrated at the bottom right, again for ^{12}C + Ne, and they are certainly well developed by 91 MeV/nucleon[27]) (see example for ^{12}C in an emulsion, top right). It is likely that these high multiplicity events are the result of central collisions. In an attempt to focus on these processes we describe in the next section, experiments on light particle emission with a central collision trigger, in which simple processes of projectile fragmentation, excitation and decay are excluded.

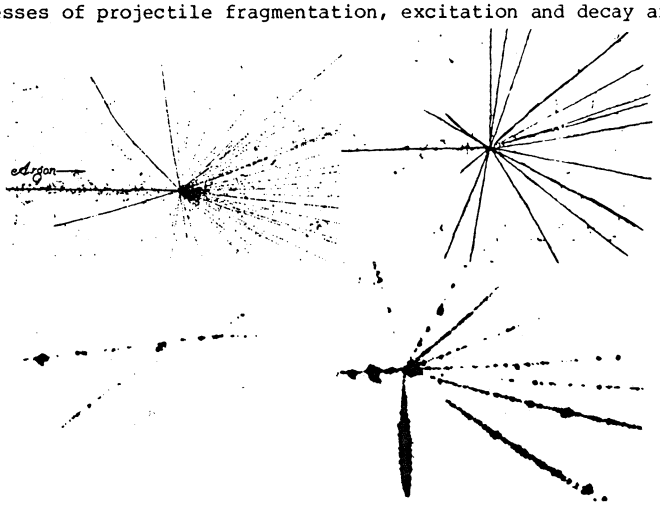

FIG. 7. Streamer Chamber (lower) and emulsion (upper) photographs of events in heavy-ion collisions. Bottom frames show examples of few and many particle final states for ^{12}C + ^{20}Ne at 25 MeV/nucleon. Top frames illustrate explosive events with ^{40}Ar at 1.8 GeV/nucleon (left) and ^{12}C at 81 MeV/nucleon (right).

3. Systematics of light particle production

A useful trigger for central collisions in heavy-ion collisions at energies in the vicinity of 10 - 20 MeV/nucleon is illustrated[28-30]) in fig. 8. The light particles are detected in a ΔE - E telescope in coincidence with fission fragments from the residual heavy system. By measuring the angle θ_{AB} between the outgoing fission fragments as well as their energies, the recoil momentum can be deduced. In fig. 8 the fission coincidence spectra are shown as a function of θ_{AB} in an inclusive measurement (i.e. any particle detected in the forward telescope) as well as for coincident protons over a wide range of angles (15° to 140°). The existence of two peaks in the inclusive distribution points to two dominant momentum transfers. The peak close to 173° (corresponding to the smaller transfer) is associated with a peripheral process; it is the only peak found in coincidence with projectile-like fragments centered close to beam velocity, which are known to be produced in peripheral reactions. The large momentum transfer (θ_{AB} = 148°) is then attributed to central collisions. Clearly there is a sizeable probability for emission of fast protons above the region of evaporation in both peripheral and central collisions, but at backward angles only the central component persists. The arrows in the figure indicate the position at which the recoil momentum is equal to the difference between the mean momentum carried by the coincident light particle and the beam momentum. The reaction mechanism may therefore resemble the incomplete fusion process mentioned earlier.[23]) In a similar experiment at 86 MeV/nucleon for ^{12}C on U, shown in fig. 9, no central fission peak remains in coincidence with light particles at forward angles.[31]) The inference here is that the central collisions have led to more violent disruptions of the nucleus,[32]) a conclusion also supported

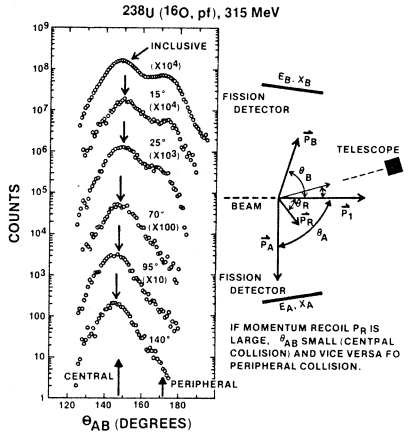

FIG. 8. Distribution of opening angle θ_{AB} of fission fragments produced in ^{16}O + U at 315 MeV for inclusive reactions (top) and in coincidence with forward fast protons at several angles.

by studies at higher energies of 400 MeV/nucleon.[33] It remains to map out this disappearance of the fission component between 20 and 86 MeV/nucleon in large momentum transfers, and to discover the mechanisms which replace it.

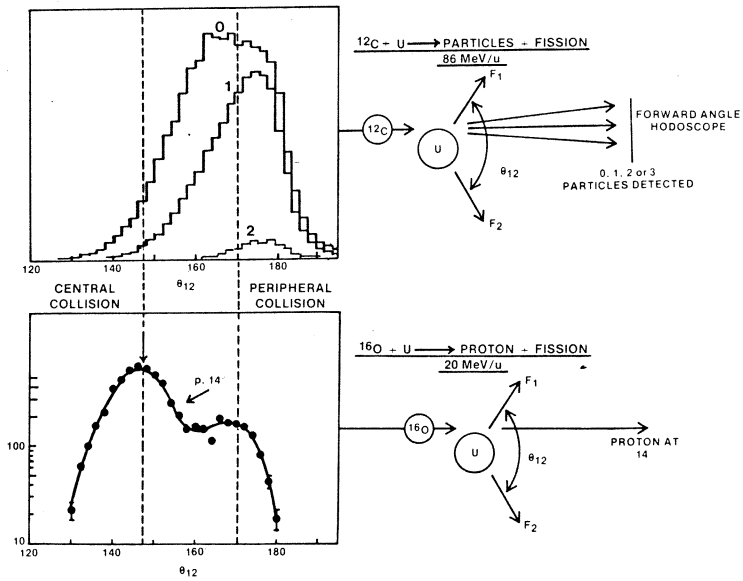

FIG. 9. Comparison of the distribution of opening angles of fission fragments in coincidence with forward going light particles for ^{12}C + U at 86 MeV/nucleon (top) and ^{16}O + U at 315 MeV (bottom).

Returning to low energies, proton spectra from ^{16}O + U at 315 MeV are shown in fig. 10. (Here contributions from peripheral and central processes are included, but beyond 40° the peripheral contribution is negligible.) It is quite clear that the spectra cannot originate from a classical compound nucleus. By extending up to energies of 80 MeV with substantial cross section they require much too high temperatures. The center of mass energy of ~200 MeV above the barrier leads to T = 2.9 MeV for the compound system, using $E^* = \frac{A}{8} T^2$, and we expect a decrease of 10^9 in cross section between 10 and 70 MeV, compared to typical observed factors of only 10^3. What type of source, one must ask, is responsible for this emission? Interpretations abound in the literature [34]) and some of them were mentioned briefly in the previous section. We note, however, that in this experiment, simple processes of projectile fragmentation and decay are ruled out.

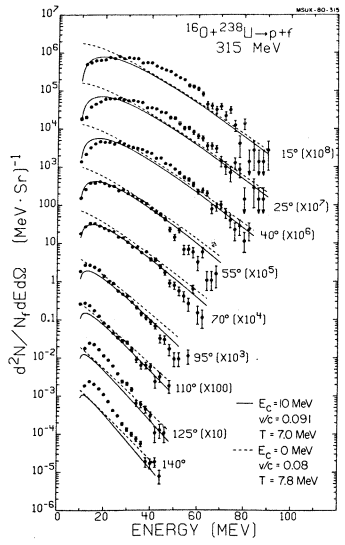

FIG. 10. Energy spectra of protons in coincidence with fission fragments for reactions of ^{16}O + U at 315 MeV. The solid line is a theoretical fit with a moving source model discussed in the text. The dashed line shows the effect of varying parameters.

To emphasize systematic features as well as to establish a link to processes occurring at much higher energies, we shall abandon all detailed theoretical models and resort to a simple parameterization of the data,[32,35]) in terms of a thermal distribution at a temperature T in a rest frame that moves with velocity v, parallel to the beam axis. After correcting for the Coulomb repulsion from the target one obtains,

$$\frac{d^2N}{d\Omega dE} = N_o (E-E_c)^{\frac{1}{2}} \exp - \left[\frac{E-E_c+E_1-2E_1^{\frac{1}{2}}(E-E_c)^{\frac{1}{2}}\cos\theta}{T} \right]$$

where E_c is the kinetic energygained by Coulomb repulsion, $E = \frac{1}{2}mv^2$ is the kinetic energy of a particle moving with the source velocity and N_o is an overall normalization constant. The solid curves are calculated with E_c = 10 MeV, v = 0.09c and T = 7 MeV. The velocity is close to half the beam velocity, if the slowing down of the projectile in the field of the target is taken into account. The occurrence

of sources moving with approximately half the beam velocity is observed in many other systems[36]).

Compare now results for proton emission in much higher energy reactions of Ne on NaF at 400 and 800 MeV/nucleon [37]) in fig. 11. The relativistic generalization of the above equation,

$$\frac{Ed^2\sigma}{p^2dpd\Omega} = N_o\,(E-\beta p\cos\theta)\exp\left[-\gamma(E-\beta p\cos\theta)/T\right]$$

with

$$\beta = v/c,\ E = (p^2+m^2)^{\frac{1}{2}},\ \gamma = (1-\beta^2)^{-\frac{1}{2}}$$

is also successful in describing the high energy tails of the spectra. The fits shown are only for scattering angles greater than 45 °, providing a bias towards central collisions. The derived velocities of 0.39 and 0.46c are again approximately one half the beam velocities of 0.71 and 0.84c at 400 and 800 MeV/nucleon respectively, but much higher temperatures of 47 and 73 MeV are now produced.

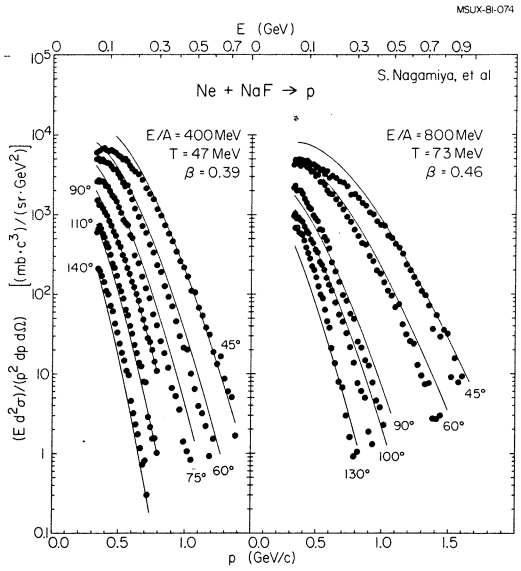

FIG. 11. Spectra of protons in the reaction Ne + NaF → p at 400 and 800 MeV/nucleon. The curves are calculated with a moving source model.

The systematic dependence of the temperatures on the incident energy per nucleon above the barrier for the above cases, as well as for other lower energy ^{16}O induced reactions, is shown in fig. 12 by the black circles. The open circles denote a similar analysis applied to tritons, and the inset shows the detailed behaviour for p, d and t in the low energy regime. The variation of T is roughly linear with $\left[(E-V_c)/A\right]^{1/2}$. If we assume that the source is composed of equal numbers of contributing nucleons from projectile and target, consistent with the derived half beam velocities, then the excitation energy per nucleon, E^*, is related to the incident energy per nucleon above the barrier, $(E-V_c)/A$ by

$$E^* = \left[m_o^2 + \tfrac{1}{2}m_o(E-V_c)/A\right]^{\frac{1}{2}} - m_o$$

where m_o is the nucleon rest mass. At low energies and temperatures we write

$$E^* = \frac{1}{8} T^2 \text{ with } E^* = \frac{1}{4} \frac{E-V_c}{A} ,$$

since $(E-V_c)/A \ll m$. The above linearity is then readily understood. In general $E^* = \langle E(T) \rangle - \langle E(T=0) \rangle$ with $\langle E(T) \rangle$ computed from the Fermi distribution function and $\langle E(T=0) \rangle = 3/5 \epsilon_F$. The resultant relation between T and $(E-V_c)/A$ up to 1 GeV/nucleon is shown in fig. 12 by the solid line, which follows the trend of the data rather well. For comparison the equivalent line for a classical Boltzmann gas is also illustrated; the two formulations are of course almost identical at high temperatures. Very recent data on proton emission from ^{12}C on Au at 86 MeV/nucleon [38]) are also consistent with emission from a source moving with half beam velocity and a temperature of about 16 MeV. The temperature fits exactly on the trend of the proton data in fig. 12.

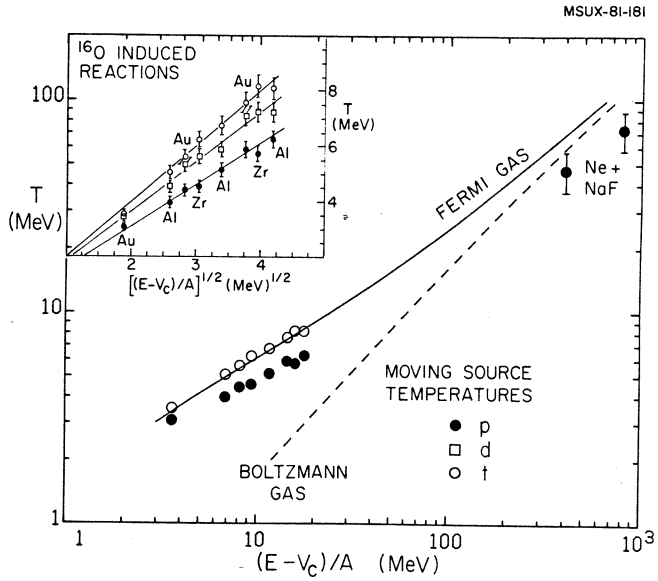

FIG. 12. Temperature parameters for proton, deuteron and triton spectra in ^{16}O induced reactions on targets of Al, Zr and Au at incident energies of 140, 215 and 310 MeV and for the reaction Ne + NaF at 400 and 800 MeV/nucleon. The curves are discussed in the text.

At present one should regard the consistency of the description over a wide energy range as indicative of common underlying reaction mechanisms, reinforcing our qualitative observations in Section 2 on the similarity of the high energy tails appearing in the corresponding neutron spectra. The extent of thermal equilibrium reached in a localised Fermi gas and the importance of single nucleon-nucleon collisions over the whole energy domain of fig. 12 remains to be established. Suffice it to say that the most rapid progress is likely to be made by keeping in mind the superficially different theoretical models that have been developed in the low and high energy limits. Some of these approaches are discussed in the next section.

4. More formal theoretical approaches

The participant-spectator model is the basis of many high energy descriptions of nuclear collisions. A source of intermediate rapidity, equal to half the beam rapidity in the case of equal mass target and projectile, is formed from the overlapping portions of the nuclei.[39]) This simple picture and its derivatives in terms of firestreaks[40]) or two fireballs,[41]) can be discussed in the more elaborate cascade[42]) and hydrodynamical models,[43]) an example of which is shown in fig. 13. The density, temperature and velocity profiles for Ne and U in a peripheral collision at 400 MeV/nucleon contain a high velocity, low density (fragmented) projectile remnant, a low velocity target spectator and an intermediate velocity zone of high temperature. It is from this participant zone that the protons of fig. 11 are believed to originate. These theories can give a description of the data comparable to, or better than, the simple parameterization of a moving source discussed earlier. Nevertheless that simple parameterization captures the spirit of the more formal approaches, and helps to focus the question of whether any remnant of this participant zone remains at low energies.

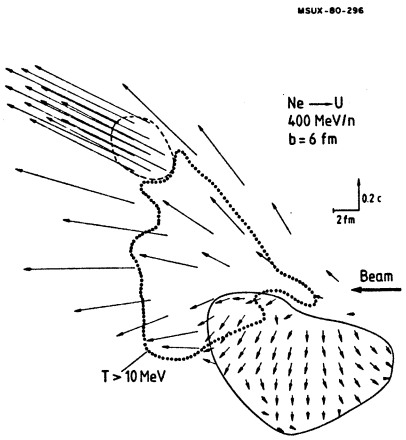

FIG. 13. Temperature, density and velocity profiles for peripheral collisions of ^{20}Ne + U at 400 MeV/nucleon in a hydrodynamical model.

If so, in all likelihood, it should be associated with the high temperature regions formed in localized hot-zone models, the schematic version of which illustrated in fig. 14 has been applied to reactions at 20 MeV/nucleon.[17]) Two spherical caps are chosen of equal thickness d, which is treated as a free parameter. For the energy of the nucleons in the zone, a Fermi gas distribution is assumed, without any compression, and from the boundaries nucleons are emitted in all directions. In the surrounding cold matter, the mean free path is long so that the particles reach the surface without absorption. However, nucleons emitted into the hot region are completely absorbed on account of the shorter mean free path. The calculated variation[44]) of λ with T is shown in fig. 15. When many particles are excited out of the Fermi sea, the effect of the Pauli exclusion principle is relaxed and two-body collisions dominate over mean field collisions with the wall. Thus, even at low incident energies, as the temperature approaches 10 MeV, the nucleon mean free path approaches the high energy classical limit of $1/\rho\sigma \approx 2$ fm. Such a reduction of the mean free path is essential for hot-spot formation, as well as for the validity of

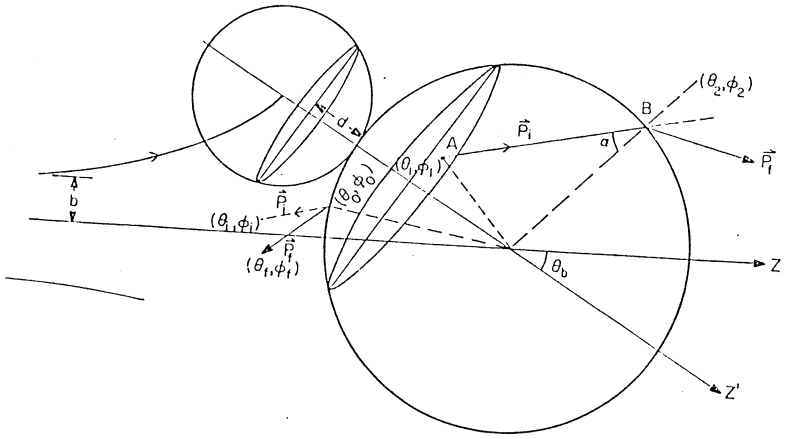

FIG. 14. Schematic model for creation of a hot zone in heavy ion collisions. The zone is parameterized by the caps of depth d, and particle emission is calculated from the surfaces of the zone.

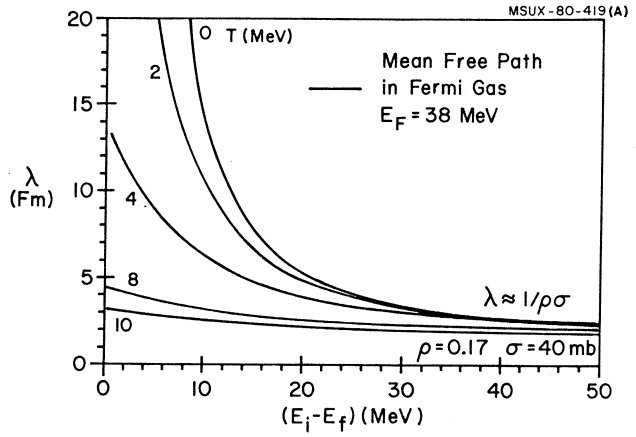

FIG. 15 Theoretical predictions of the nucleon mean free path as a function of energy above the Fermi Energy for different nuclear temperatures.

hydrodynamics. The temperature dependence helps to reconcile the concepts of hot-zone formation at low energies with the paradoxical requirement in TDHF calculations of very long mean free paths, which are more relevant at temperatures close to zero. The mean free paths shown for T = 0 are more or less commensurate with the experimental values deduced from the depth of the imaginary potential,[10]) viz.

$$\lambda = \frac{1}{W}\sqrt{\frac{(hc)^2 E}{2mc^2}} \quad .$$

However, recent experimental and theoretical results suggest that the T=0 mean free paths may be longer[45]. Other discussions of the mean free path are given in ref. 46.

The total flux of protons dN/dt is calculated and the energy spectrum $d\sigma\, dE$ is obtained by summing over impact parameters and multiplying by Δt, the time of emission from the surface of the hot zone. The results for the integrated energy spectrum of protons from ^{16}O on ^{197}Au at 310 MeV (obtained from spectra which are similar, but not identical, to those of fig. 10) appear in fig. 16(a); a value of $t = 2 \times 10^{-22}$ sec, of the order or slightly smaller than the collision time at 20 MeV/nucleon, viz $2R/v \simeq 4 \times 10^{-22}$ sec was used, with d = 2.5 fm. Results for the detailed form of the angular distributions are also found to be in moderate agreement with experiment. In an attempt to improve the agreement with the angular distribution the contribution from PEPS or Fermi jets have recently been incorporated, and the results are shown in fig. 16(b) by the dot-dash line.[47]) The contribution of PEPS to the integrated cross section comes mainly from forward angles of less than 50°, and is negligible at backward angles. It appears that although Fermi jets may play an important role at energies of a few MeV/nucleon, they are secondary to the hot-spot mechanism at 20 MeV/nucleon and higher. This observation reinforces our earlier remarks on comparing the high energy tails of different neutron spectra (fig. 5) that an interpretation based on the occurrence of no collisions was unlikely.

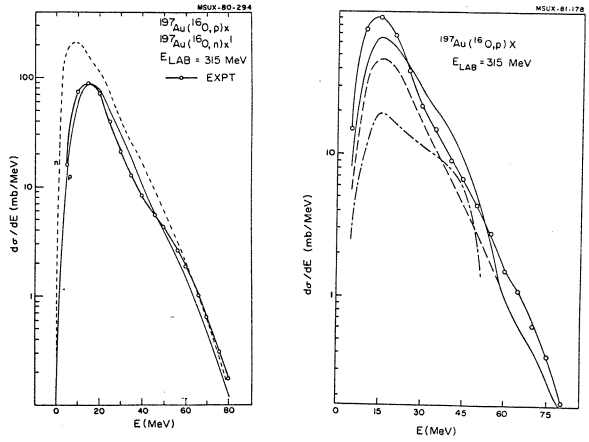

FIG. 16. (a) Angle integrated energy spectrum for nucleons emitted in $^{16}O + ^{197}Au$ at 315 MeV. The thin solid and dashed curves are hot-spot model predictions; (b) comparison of data with hot-spot model (dashed), PEPS (dot-dash) and the combination (solid line).

More elaborate hot-spot theories are also developed[19,20,48]) in which the classical heat transport equation,

$$\frac{\partial}{\partial t} T(r,t) = 1/\rho c_p \quad \nabla\cdot(K\, T(r,t))$$

is solved for the temperature field T, where ρ is the nuclear density, K the thermal conductivity and c_p is the specific heat of nuclear matter. The quantity K, like the mean free path, is itself temperature dependent. The theory predicts asymmetries in

the emission pattern of the light particles from the zone. Although there is some evidence for this behaviour already at low energies of 5 MeV/nucleon,[49]) perhaps the most convincing experiment and theoretical analysis come from the realm of high energy hadronic reactions. Here it is conjectured that high energy pions may be evaporated from a hadron after the localized excitation has started to propagate but before the energy is spread evenly over the hadron. The effect has been searched for[50]) in the reaction $K^- + p \rightarrow K^- p \pi^+ \pi^-$ at 14 GeV/c. According to the diagram in fig. 17, more high energy pions should be radiated from the hot spot formed at the south pole than from the north pole. The distribution as a function of $\cos\theta$ appears to contain such an effect, whereas the ϕ distribution has no asymmetry. Experiments of this type are being used to determine the relaxation time constants of hadronic

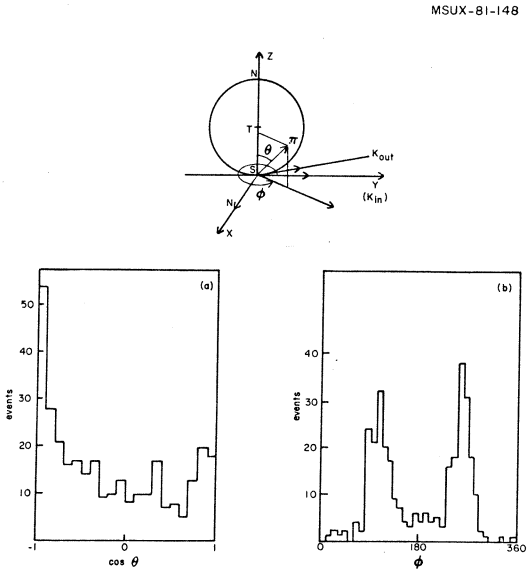

FIG. 17. Schematic representation of pion production from hadronic, hot spot for the reaction $K^- p \rightarrow K^- p \pi^+ \pi^-$ at 14 GeV/c. The distributions of pions in polar angles ($\cos\theta$) and in azimuth (ϕ) are shown in (a) and (b).

and nuclear matter,[51]) although few results are available in cases of heavy-ion collisions. In fact it seems that most coincidence measurements between light and heavy fragments, which are necessary to establish the asymmetry, can be explained using other mechanisms, such as projectile fragmentation or delayed fragmentation,[21]) and orbiting of deep-inelastic fragments.[52]) However, our understanding of the coincidence experiments at present is far from complete[53],[54]). Experiments on backward production of light particles also show many similarities at low and at very high energies. Thus the 180° emission of protons in reactions of 90 MeV protons on various targets,[55]) and in reactions induced by protons between 0.6 and 400 GeV have been analysed with hot-spot models.[56]) There are also more mundane interpretations based on fragmentation models[57]) or on the exponentially falling virtual momentum spectrum of nucleons in nuclei.[58])

By way of contrast we conclude this section with a brief mention of microscopic models which can be used to describe the high energy tails of energy spectra. Underlying all such calculations is the idea of a sequence of nucleon-nucleon

collisions generating a hierachy of excitations. In the intranuclear cascade,[42,59]) the trajectory of each nucleon is followed, and, after one mean free path, a collision takes place, the result of which is computed by Monte Carlo methods. In the exciton formulation, the nuclear shell model is the basis of the approach.[7]) A master equation is derived, describing how the target-projectile system develops in the space of particle-hole configurations. A third approach using DWBA and CCBA has also been followed,[60]) inferring that a few inelastic collisions can often suffice to describe pre-equilibrium spectra.

In the master equation approach, it is necessary to know the number of excitons in the initial channel and there exists a well established prescription in light-ion reactions.[61]) The cross section for emission of particle β is written,

$$\frac{d\sigma_\beta(E)}{dE} \propto E\,\sigma_\beta(E)\; U^{p+h-\beta-1}$$

where U is the excitation energy of the residual nucleus, σ_β is the inverse cross section for particle β at energy E. Then a plot of $\log\left[d\sigma_\beta(E)/EdE\right]$ vs σ_β a function of log U gives the slope S = p + h - β - 1, where p + h is the number of particles and holes. Examples are given in fig. 18 for d and α-induced reactions;[62]) the associated number of particles and holes (p + h) is 4 (i.e. 3 particle - 1 hole), and 6 (5 particle - 1 hole) respectively, since the initial interaction creates a particle-hole state which then combines with the nucleons of the incident particle. The same analysis applied to ^{16}O as a projectile leads us to expect at least 18 excitons; in fact the same graphical analysis[63]) gives 25. Angular distributions calculated with this exciton model have also given a plausible account of proton data of the type shown in fig. 10.

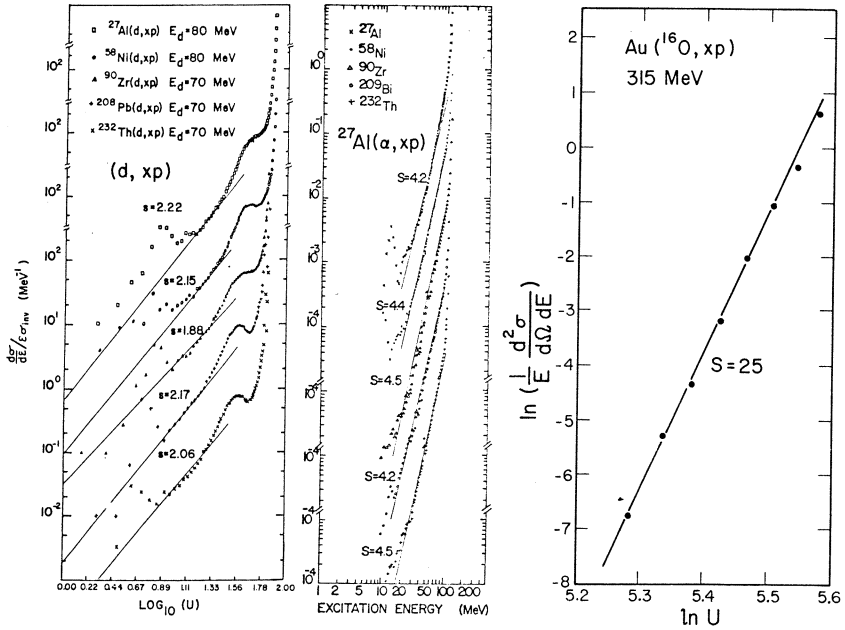

XBL 7811-13171

FIG. 18. Analysis of d, α and ^{16}O induced reactions leading to light particle pre-equilibrium emission to determine the number of contributing excitons (p+h) from the slope (S), of $\left[\frac{d\sigma_\beta}{dE} / E\sigma_\beta\right]$ vs. log (U) as discussed in the text.

The relationship between the multi-exciton state of the microscopic model and the localized hot zone of the macroscopic model is certainly not transparent. We note, however, that the concept of temperature, while meaningless for the few-exciton states created in hadron reactions, may be definable for the heavy-ion reaction, where the initial number is large and does not change appreciably in the course of the high energy particle emission. In the next section we present some other considerations on the size of the hot zone that may be formed when heavy-ions collide.

5. Size of the hot zone

It is instructive first to use geometrical considerations[39] in deducing the size of the participant zone formed in high energy heavy-ion collisions (recall fig. 13). The average number of participants which come from the beam nucleus $\langle Z_B^P \rangle$ can be calculated as follows. If a proton in the projectile hits the target it becomes a participant:

$$\langle Z_B^P \rangle = Z_B \pi r_o^2 A_T^{2/3} / \sigma_R$$

where σ_R is the reaction cross section. Similarly

$$\langle Z_T^P \rangle = Z_T \pi r_o^2 A_B^{2/3} / \sigma_R \ .$$

Thus the total charge multiplicity of the participants is

$$\frac{Z_T A_B^{2/3} + Z_B A_T^{2/3}}{(A_B^{1/3} + A_T^{1/3})^2}$$

For the case ^{20}Ne + U, the value is 13, which is shown on the charged particle multiplicity plot in fig. 3. The observed multiplicities at high energies are of this order; in the more sophisticated treatment of the nuclear firestreak model,[49] the multiplicity becomes a function of the incident energy, following the trend of the experimental data.[64] The number of participant neutrons is comparable but slightly higher, and the total number of participant particles is ≈30. This number may be compared to the number of excitons in the microscopic models, if the geometry of the localized zone is the same at low and high energies. We recall that in the hot-spot model (fig. 14) the zone was computed[17] with end caps of d = 2.5 fm. The associated volume is 163 fm^3, containing 28 particles. Referring to fig. 3, one can speculate that the multiplicity will approach the participant limit at an energy where the system can be completely disassembled. Although the correspondences at this stage may be coincidental, it is interesting to note that similar source sizes arise in the analysis of composite particle production, as discussed below.

There are two current approaches to the production of light composite particles in heavy-ion collisions. The coalescence model[65] determines the probability for condensation of nucleons, which takes place if they lie within a coalescence radius p_o. The probability of finding a nucleon in a sphere of radius p_o centered at p is:

$$P \approx (\tfrac{4}{3}\pi p_o^3) \ \frac{d^2\sigma_1(p)}{p^2 dp \ d\Omega}$$

where $d\sigma_1(p)/p^2 dp d\Omega$ is the cross section for emission of a single nucleon. Then the probability for finding A nucleons is just,

$$P_A \approx (\tfrac{4}{3}\pi p_o^3)^A \left[\frac{d^2\sigma_1(p)}{p^2 dp d\Omega}\right]^A$$

To obtain the cross section, we take the probability of finding A-1 nucleons in the sphere p_o, multiplied by 1/A times the cross section for the emission of an additional particle. The final expression takes the form,

$$\frac{d^2\sigma_A}{p^2 dp d\Omega} \approx \frac{1}{A!} \left(\frac{4\pi p_o^3}{3\sigma_o \gamma}\right)^{A-1} \left[\frac{d^2\sigma_1}{p^2 dp d\Omega}\right]^A$$

where σ_o is the reaction cross section and γ is the relativistic correction factor. Once the cross section for single nucleon emission is known, the cross section for composite fragments is determined with only one additional parameter p_o.

This power law dependence is however also expected in a thermodynamic model.[66] Then the cross section for fragment emission is given by exp (-E/T) which can be written,

$$\left[\exp\left(\frac{-E/A}{T}\right)\right]^A$$

i.e. the single nucleon cross section raised to power A at the same MeV/nucleon. In spite of this equivalence, the physical content of the models is superficially different (although in a more sophisticated treatment[67], they can be shown to be more closely related). The coalescence radius is an intrinsic property of the emitted particle and consequently should be independent of energy and mass of the

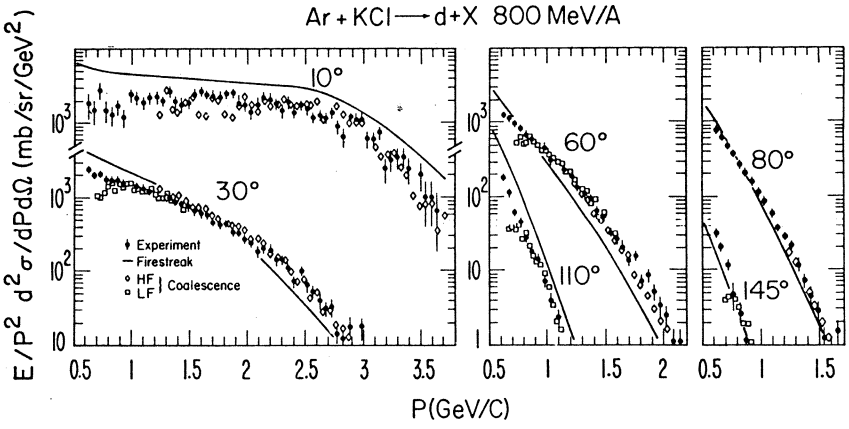

FIG. 19. Comparison of momentum spectra for deuterons, produced in the reaction Ar + KCl at 800 MeV/nucleon, with the coalescence model. The solid line compares the firestreak prediction.

colliding system. The equivalent constant of the thermodynamic model is related to the volume in which thermodynamic and chemical equilibrium is established. As such it is a property of the emitting region and will depend on the size of the nuclei forming it.[68] (Again, in a more thorough analysis[69] the two effects must be folded together, i.e. there is a dependence on initial and final state interactions.) Apart from numerical constants the parameters of the two models are related by

$$V \propto h^3/p_o^3$$

The power law dependence is followed rather closely at relativistic energies,[65] as illustrated in fig. 19 by the reaction $^{40}Ar + {}^{208}Pb \rightarrow d$ at 800 MeV/nucleon with a coalescence radius of 213 MeV/c. Expressing the thermodynamic volume in terms of the radius of an equivalent shpere, values of R equal to 3.7 fm are typical. The prescription works over a wide variation of incident energy and colliding nuclei, including α particles in the initial channel, and even complex fragments like ^6Li in the final channel.[70]

The interesting physics comes from the trends of the parameters as a function of energy or mass. In fig. 20 we show how the radius R (as defined above) depends on $(A_P^{1/3} + A_T^{1/3})$ for many different colliding systems at widely varying energies. The vertical bars represent the range of values derived for different emerging particles, typically protons to alphas. Results are included for α-particle induced reactions[70]) at 25 MeV/nucleon, for the ^{16}O induced reactions[29,30]) at 20 MeV nucleon which have been frequently discussed in this paper, and for results at relativistic bombarding energies of 400 - 2100 MeV/nucleon for many systems.[65]) There is a tendency for the radius to increase with $A_P^{1/3} + A_T^{1/3}$, favoring the thermodynamic interpretation. We must note however that other results for light particle induced reactions, analyzed with a more microscopic model,[71]) are less supportive of this interpretation. From fig. 20, however, we conclude that if the emission of complex fragments originates from chemical equilibrium in a localized source, then the radius is typically 3.5 fm; once again it is associated with about 30 particles.

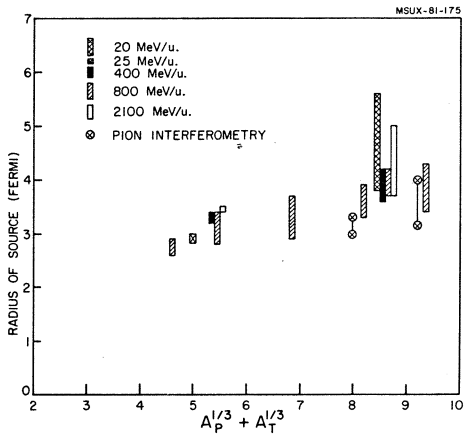

FIG. 20. Variation of effective source size produced in heavy-ion collisions as a function of $(A_P^{1/3} + A_T^{1/3})$, deduced from composite light particle production. Two results from pion interferometry are also shown.

As a final piece of evidence on source sizes, we mention the more direct determination of the space-time geometry by means of two-particle intensity interferometry.[72,73]) Results from experiments on detected pions are also shown in fig. 20 and are consistent with the source radii determined from the emission of composite particles. It is less clear, however, that results with two proton interferometry present a consistent picture of the size of the participant region.[74]) The method of interferometry will no doubt be applied soon over a wide energy range to determine source sizes. In addition to this application, it can also yield information on the degree of coherence or chaoticity in the source, and thereby on possible exotic conditions.[75]) Some of the exotic possibilities, as revealed by means of light particle emission in heavy-ion reactions, are discussed in the last section.

6. Exotic considerations

Light particle production may offer a means of determining the entropy created in the source. An excess of entropy over that produced by normal processes could indicate other degrees of freedom, such as might come about from a phase transition to a pion condensate or to quark matter. It has been suggested that the deuteron to proton ratio might convey information about the entropy in the intial, hot participant zone.[76]) According to recent calculations,[77]) the subsequent hydrodynamic expansion of the zone creates little additional entropy, of the order of 0.5 units. The ratio of deuterons to protons reaching the detectors is therefore a measure of the entropy in the final phase of the reaction where the deuterons are constantly forming and breaking up. A small number of deuterons points to large entropy and vice versa. The expected entropy per baryon of a Fermi gas as a function of energy/nucleon is shown[77]) in fig. 21. At low energies it has the form $S = (\pi^2/2\epsilon_F)\,T$, whereas at high energies it varies as $\ell n\ T$ characteristic of a classical gas. The variation is shown for two cases of viscous (S_η) and inviscid (S_s) systems. Also shown are the experimental specific entropies[78]) for the Ne + NaF system at 400 and 2100 MeV/nucleon, calculated from

$$S = 3.95 - \ell n \frac{\langle d \rangle}{\langle p \rangle}$$

More entropy is generated than can be accounted for in the calculation, a result which is also borne out by Monte Carlo cascade calculations.[79]) The discrepancy has been attributed to the presence of other unknown degrees of freedom in the participant zone.[76]) A more recent analysis explains the excess of entropy in terms of pion production,[80]) but other hydrodynamic calculations continue to produce a discrepancy.[81])

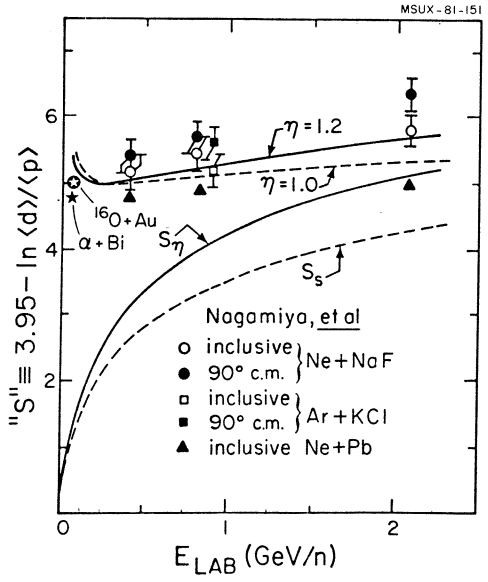

FIG. 21. Measured entropy deduced from the deuteron to proton ratio for several reactions as a function of energy/nucleon. The theoretical curves are the predictions of hydrodynamical models, as discussed in the text.

A note of caution over the interpretation of this discrepancy must be injected. In fig. 21, the function S is also plotted for data on the same system Ne + NaF at a lower energy of 400 MeV/nucleon.[78]) Here, of course, the functional form pertaining to a classical gas is not relevant, since the temperatures are low enough for Fermi and Bose statistics to act. Nevertheless, the surprising result is that the deuteron to proton ratio, and hence the functions derived from it, does not change very much over the entire energy range. This observation is more dramatic for the system Ne + Pb which is also shown,[78]) and can be compared with the ^{16}O + Au results at even lower energies of 20 MeV/ nucleon.[30]) Even data for the α+ Bi system at 25 MeV/nucleon follows the trend.[82]) The uniform behaviour is apparently contained in a hydrodynamic calculation,[77]) which includes the decay of excited states of the light composite particles. These increase the proton population and effectively reduce the <d>/<p> ratio from the primary values related to the entropy. The hydrodynamical model predictions of "S", which are now no longer a direct measure of entropy, is shown for viscous and inviscid conditions. There are also recent speculations[83]) that the deuteron to proton ratio may be limited by the exclusion principle at low energies, providing an independent explanation of the ratio of 0.3. We should point out that the results for α + Bi, Ne + Pb and ^{16}O + Au are derived from inclusive measurements and may be contaminated by deuteron production from processes originating outside the participant zone. Some indications of the possible differences are shown in fig. 21 by comparing the inclusive and the 90° cm results which emphasize the intermediate rapidity fireball region, for the system Ne + NaF. In general deuterons can be generated not only by participant-participant interactions in the fireball zone, but also by participant-spectator interactions,[84]) or by a "snowball" mechanism[85]) in which a nucleon suffers a collision and then gathers up one or more nucleons on the way out.

Another exotic aspect of localised hot zones, accessible through light particle emission, concerns their disintegration at high temperature.[86]) When the excitation energy per nucleon in an interacting volume of nucleons composed of a_1 nucleons from the projectile and a_2 from the target, viz.,

$$E^* = E_{LAB} \frac{a_1 a_2}{(a_1+a_2)^2}$$

exceeds 8 MeV, the average binding energy per nucleon, the system will disintegrate.[27]) If equal numbers of nucleons from projectile and target participate, $a_1 = a_2$ and $E_{LAB} = 32$ MeV/nucleon. The results of a more refined calculation,[86]) with proper treatment of surface and volume effects, are shown in fig. 22. The volume energy per particle as a function of compression $\eta = \rho/\rho_o$ at different temperatures is plotted, and is close to zero for T = 18 MeV with η = 1.3. According to the systematics of fig. 12, the required energy/nucleon is then $\approx$50 MeV/nucleon. A high multiplicity of nucleons should then be emitted from the zone. It is tempting to attribute the onset of this effect to the behaviour exhibited in fig. 3, but more detailed studies are necessary over the important energy region from 20 - 100 MeV/nucleon. This type of study could yield results relevant to the determination of the equation of state. The disintegration of nuclear systems has also been investigated in the TDHF method, in which the overlapping region of the two nuclei produces a rapid increase in the density and an associated increase in the mean field potential.[87]) The resultant "volcano effect" makes the nucleons become unbound.[88])

7. Conclusions

The emission of fast light particles is certainly an important process in nuclear collisions at incident energies of 20 MeV/nucleon and above. It conveys information about reaction mechanisms that differ considerably from the global equilibrium reached in low energy compound nuclear and deep-inelastic scattering. In particular the light particle emission is one of the best sources of information on the progress of the system towards that equilibrium. At present a variety of theoretical models exist to describe the pre-equilibrium emission. These range from

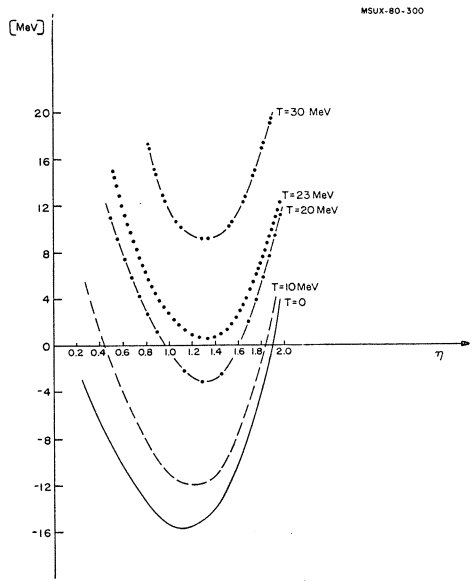

FIG. 22. The volume energy of nuclear matter per particle as a function of compression η at different temperatures T.

microscopic processes of the intranuclear cascade, the master equation, the DWBA and CCBA, to macroscopic theories of the participant-spectator mechanism and nuclear hydrodynamics. These approaches tend to emphasize a few nucleon-nucleon collisions on the one hand, and many collisions leading to local thermal equilibrium on the other. There is, however, an increasing awareness that many nucleon collisions could also be important in the low energy regime, just as one or two nucleon processes play a role at high energies. In the absence of detailed calculations with a complete theory, various simple approaches are adopted. Thus some aspects of the low energy data are interpreted with hot-spot models, which may be related to the localized participant zone at high energies. Systematics in the experimental data are suggestive that a local high temperature source exists. Definitive proof is awaited but is certainly important, because the existence of this zone is closely linked to a short mean free path for nucleons in heavy-ion collisions, a condition which must also be met if nuclear hydrodynamics is to be a useful approach. On more formal grounds, an understanding of the high energy pre-equilibrium spectra should clarify the importance of collision terms, beyond the usual mean field approximation of the TDHF. At present the evidence, as presented in this paper, is suggestive but circumstantial. Often the data can also be understood using other models; in particular when more exclusive measurements are undertaken, they are usually dominated by simpler mechanisms of projectile fragmentation, delayed fragmentation or incomplete fusion.

The production of composite light particles may be a promising means of gaining information on the entropy created in heavy-ion collisions. At present there are difficulties in understanding the apparent excess at high energies; it may be indicative of exotic processes. However there are problems in understanding the production of light composite particles even at low energies, raising the questions on the high energy interpretations. The relative abundance of nucleons and light composite particles can also be used to study the disintegration of hot zones in

nuclear matter. These aspects of light particle emission are connected with the nuclear equation of state.

The idenification of the effects discussed in this paper is predicated on the formation of localized, high temperature regions in nuclear collisions. At present we have only indirect, circumstantial evidence for such phenomena. Nevertheless, whatever the outcome, it is clear that light particles are potentially a copious source of information on many details of the reaction. In this paper the emphasis was placed on the value of looking at the interactions of nuclei systematically over a wide energy region. In this way it becomes easier to spot both the similarities and the differences, the need for new reaction mechanisms in addition to the old established ones.

Acknowledgements

I am grateful to T.C. Awes, G.F. Bertsch, C.K. Gelbke, and P.J. Siemens for many useful discussions. It is a pleasure to thank Betty Brewer and Patricia Pirnie for typing and assembling the manuscript. The preparation of this paper was supported by the National Science Foundation under Grant No. Phy 78-22696.

References

1. D.Hilscher, J.R. Birkelund, A.D. Hoover, W.U. Schroder, W.W. Wilcke, J.R. Huizenga, A.C. Mignerey, K.L. Wolf, H.F. Breuer and V.E. Viola, Phys. Rev. C 20 (1979) 576.
2. I. Tserruya, A. Breskin, Z. Fraenkel, S. Wald, R. Bock, M. Dakowski, A. Gobbi, H. Sann, R. Bass, G. Kreyling, R. Renfordt, K. Stelzer and U. Arit, Weizmann Phys. Rev. Lett. 47 (1981) 16.
3. D. Hilscher, this conference.
4. J. Kasagi, S. Saini, T.C. Awes, A. Galonsky, C.K. Gelbke, G. Poggi, D.K. Scott, K.L. Wolf and R. Legrain, Michigan State University Preprint MSUCL-352 (1981), to be published in Phys. Lett. B.
5. This feature of the multiplicity was pointed out to me by K. Wolf.
6. M. Blann, Phys. Rev. C 23 (1981) 205.
7. W. Norenberg and H.A. Weidenmuller, in Lecture Notes in Physics 51 (Springer-Verlag, 1980) p 232.
8. W. Schimmerling, J.W. Kast, D. Orthendahl, R. Madey, R.A. Cecil, B.D. Anderson and A.R. Baldwin, Phys. Rev. Lett. 43 (1979) 1985; J.D. Stevenson, Phys. Rev. Lett. 45 (1980) 1773.
9. A. Galonsky, T. Amos and R.J. Jolly, Private communication, 1981.
10. H.C. Chiang and J. Hufner, Nucl. Phys. A349 (1980) 466.
11. J. Cugnon, Phys. Rev. C 23 (1981) 2094.
12. M. Chemtob and B. Schurmann, Nucl. Phys. A336 (1980) 508.
13. H. Feshbach, A. Kerman and S.E. Koonin, Ann. Phys. 125 (1980) 429.
14. R.P. Schmidt, G.J. Wozniak, G.U. Rattazzi, G.J. Mathews, R. Regimbart and L.G. Moretto, Phys. Rev. Lett. 46 (1981) 522.
15. J.P. Bondorf, J.N. de, G. Fai, A.O.T. Karvinen, B. Jacobsson and J. Randrup, Nucl. Phys. A333 (1980) 285.
16. H. Stocker, R.Y. Cusson, J.A. Maruhn and W. Greiner, Phys. Lett 101B (1981) 379.
17. W.W. Morison, S.K. Samaddar, D. Sperber and M. Zielinska-Pfabe, Phys. Lett. 93B (1980) 279 and ref. therein.
18. P. Mooney, W.W. Morison, S.K. Samaddar, D. Sperber and M. Zielinska-Pfabe, Phys. Lett. 98B (1981) 240.
19. P.A. Gottschalk and M. Westrom, Nucl. Phys. A314 (1979) 232.
20. R. Weiner and M. Westrom, Nucl. Phys. A256 (1977) 282.
21. W.A. Friedman and P. Saloner, Phys. Rev. C23 (1981) 2532 and refs. therein.

22. J. Van Driel, S. Gonggryp, R.V.F. Janssens, R.H. Siemssen, K. Siwek-Wilczynska and J. Wilczynski, Phys. Lett. 98B (1981) 351.
23. J. Wilczynski, K. Swiek-Wilczynska, J. Van Driel, S. Gonggryp, D.C.J.M. Hageman, R.V.F. Janssens, J. Lukasiak and R.H. Siemssen, Phys. Rev. Lett. 45 (1980) 606 and refs. therein.
24. R.K. Bhowmik, E.C. Pollacco, N.E. Sanderson, J.B.A. England and G.C. Morrison, Daresbury Preprint DL/NUC/P 123E (1980), to be published in Nucl. Phys. A.
25. K. Van Bibber, W. Pang, M. Avery and E. Bloemhof, Proc. of Symposium on Heavy Ion Physics from 10 to 200 MeV/nucleon, Brookhaven Nat. Lab. Report BNL51115 (1979) p 365.
26. Various examples are given by L.S. Schroeder, Nucl. Inst. and Meth. 162 (1979) 395.
27. J.P. Bondorf, Proc. of Conf. on Large Amplitude Nuclear Motion, Lake Balaton (1979) p. 482.
28. T.C. Awes, C.K. Gelbke, B.B. Back, A.C. Mignerey, K.L. Wolf, H. Breuer, V.E. Viola and W.G. Meyer, Phys. Lett. 87B (1979) 43.
29. T.C. Awes, C.K. Gelbke, G. Poggi, B.B. Back, B. Glagola, H. Breuer, V.E. Viola and T.J.M. Symons, Phys. Rev. Lett. 45 (1980) 513.
30. T.C. Awes, G. Poggi, C.K. Gelbke, B.B. Back, B.G. Glagola, H. Breuer and V.E. Viola, Michigan State University Preprint MSUCL-343 (1980).
31. U. Lynen, Private communication (1980).
32. D.K. Scott, Nucl. Phys. A 354 (1981) 375.
33. W.G. Meyer, H.H. Gutbrod, Ch. Lukner and A. Sandoval, Phys. Rev. C 22 (1980) 179.
34. U. Schroder, Continuum Spectra on Heavy Ion Reactions, edited by T. Tamura, J.B. Natowitz and D.H. Youngblood (Harwood Academic Publishers, 1980) p. 19.
35. T.C. Awes, G. Poggi, S. Saini, C.K. Gelbke, R. Legrain and G.D. Westfall, Michigan State University Preprint MSUCL351 (1981), to be published in Phys. Lett. B.
36. A. Gavron, R.L. Ferguson, F.E. Obenshain, F. Plasil, G.R. Young, G.A. Petitt, K.A. Geoffroy; D.G. Sarantites and C.F. Maguire, Phys. Rev. Lett. 46 (1981) 8 and refs. therein; see also F. Plasil, Proc. of the Winter School (Bormio, 1981).
37. S. Nagamiya, M.C. Lemaire, E. Moeller, S. Schnetzer, G. Shapiro, H. Steiner and I. Tanihata, Lawrence Berkeley Laboratory Report LBL-12123, to be published in Phys. Rev. C.
38. B. Jacobsson, L. Carlen, P. Kristiansson, H.A. Gustafsson, T. Johansson, H. Ryde, G. Tibell, J.P. Bondorf, G. Fai, A.O.T. Karvinen, O.B. Nielsen, M. Buenerd, J. Cole, D. Lebrun, J.M. Loiseaux, P. Martin, R. Ost, C. Guet, E. Monnand, J. Mougey, H. Nifenecker, P. Perring, J. Pinston, C. Ristori and F. Schussler, Phys. Lett 102 B (1981) 121.
39. S. Nagamiya and D.J. Morrissey, Lawrence Berkeley Laboratory Preprint, 1980.
40. W.D. Myers, Nucl. Phys. A 296 (1978) 177.
41. S. Das Gupta, Phys. Rev. C 18 (1978) 2773.
42. J. Cugnon, Phys. Rev. C 22 (1980) 1885.
43. H. Stocker, J.A. Maruhn and W. Greiner, Phys. Rev. Lett. 44 (1980) 725.
44. M.T. Collins and J.J. Griffin, Nucl. Phys. A 34 (1980) 863.
45. J.W. Negele and K. Yazaki, Phys. Rev. Lett. 47 (1981) 71
46. S.I.A. Garpman, D. Sperber and M. Zielinska-Pfabe, Nuov. Cim 57B (1980); K. Muller, Phys. Lett. 93B (1980) 247.
47. P. Mooney, W.W. Morison, S.K. Samadder, D. Sperber and M. Zielinska-Pfabe, Phys. Lett. 98B (1981) 240.
48. R.M. Weiner, Phys. Rev. D 13 (1976) 1363; Phys. Rev. Lett. 32 (1974) 630.
49. H. Ho, R. Albrecht, W. Dunnweber, G. Graw, S.G. Steadman, J.P. Wurm, D. Disdier, V. Rauch and F. Schiebling, Z. Phys. A283 (1977) 235.
50. J. Goldberg, Phys. Rev. Lett. 43 (1979) 250.
51. R. Weiner, Proc. of Int. Workshop on Reaction Models for Continuous Spectra of Light Particles, Bad Honnef, 1978, edited by J. Ernst.
52. W. Dunnweber and K.M. Hartmann, Phys. Rev. Lett. 44 (1980) 729.

53. H. Ho, P. Gonthier, M.N. Namboodiri, J.B. Natowitz, L. Adler, S. Simon, K. Hagel, R. Terry and A. Khodai, Phys. Rev. Lett. 44 (1980) 1387.
54. M. Bini, C.K. Gelbke, D.K. Scott, T.J.M. Symons, P. Doll, D.L. Hendrie, J.L. Laville, J. Mahoney, M.C. Mermaz, C. Olmer, K. Van Bibber and H.H. Wieman, Phys. Rev. C 22 (1980) 1945.
55. N.S. Wall, J.R. Wu, G.C. Chang and H.D. Holmgren, Phys. Rev. C 20 (1979) 1079.
56. N. Stelte and R.M. Weiner, Proc. of XX Int. Conf. on High Energy Physics, Madison, 1980.
57. C.M. Ko and M. Ta-Chung, Phys. Rev. Lett. 43 (1979) 994.
58. R.H. Landau and M. Gyulassy, Phys. Rev. C 19 (1979) 149.
59. Y. Yariv and Z. Fraenkel, Phys. Rev. C 20 (1979) 2227.
60. T. Tamura and T. Udagawa, Phys. Lett. 71B (1977) 274.
61. J.J. Griffin, Phys. Lett. 24 B (1967) 5.
62. J.R. Wu, C.C. Chang and H.D. Holmgren, Phys. Rev. C 19 (1979) 370, 659 and 698.
63. T.J.M. Symons, P. Doll, M. Bini, D.L. Hendrie, J. Mahoney, G. Mantzouranis, D.K. Scott, K. Van Bibber, Y.P. Viyogi, H.H. Wieman and C.K. Gelbke, Phys. Lett. 94B (1980) 131.
64. S. Sandoval, H.H. Gutbrod, W.G. Meyer, A.M. Poskanzer, R. Stock, J. Gosset, J.-C. Jourdain, C.H. King, G. King, Ch. Lukner, Nguyen Van Sen, G.D. Westfall and K.L. Wolf, Phys. Rev. C 21 (1980) 1321.
65. M.C. Lemaire, S. Nagamiya, S. Schnetzer, H. Steiner and I. Tanihata, Phys. Lett. 85B (1979) 38.
66. A. Mekjian, Phys. Rev. Lett. 38 (1977) 640; Phys. Rev. C 17 (1978) 1051; Phys. Lett. 89B (1980) 177.
67. B.K. Jennings, S. Das Gupta and N. Mobed, Preprint 1981.
68. S. Das Gupta and A. Mekjian, Phys. Reports, to be published.
69. H. Sato and K. Yazaki, Phys. Lett. 98B (1981) 153.
70. G. Gaul, R. Glasow, H. Lohner, B. Ludewight and R. Santo, private communication; H. Lohner, B. Ludewigt, D. Frekers, G. Gaul and R. Santo, Z. Phys. A292 (1979) 35.
71. H. Machner, Phys. Rev. C 21 (1980) 2695; Phys. Lett. 96B (1979) 129.
72. S.Y. Fung, W. Gorn, G.P. Kiernan, J.J. Lu, Y.T. Oh and R.T. Poe, Phys. Rev. Lett. 41 (1978) 1592.
73. J. Bartke, Proc. of the Int. Conf. on Nuclear Physics (abstracts), Lawrence Berkeley Laboratory Report LBL-11118, p. 537.
74. F. Zarbakhsh, A.L. Sagle, F. Brouchard, T.A. Mulera, V. Perez-Mendez, R. Talaga, I. Tanihata, J.B. Carroll, K.S. Ganzer, G. Igo, J. Oostens, D. Woodward and R. Sutter, Phys. Rev. Lett. 46 (1981) 1268.
75. M. Gyulassy, S.K. Kauffmann and L. Wilson, Phys. Rev. C 20 (1979) 2267.
76. P.J. Siemens and J.I. Kapusta, Phys. Rev. Lett. 43 (1979) 1486.
77. H. Stocker, Lawrence Berkeley Laboratory Preprint LBL-12302 (1981).
78. S. Nagamiya, M.-C. Lemaire, E. Moeller, S. Schnetzer, G. Shapiro, H. Steiner and I. Tanihata, Lawrence Berkeley Laboratory Preprint LBL-12123, to be published in Phys. Rev. C.
79. G.F. Bertsch and J. Cugnon, Proc. of 5th High Energy Heavy Ion Summer Study (Berkeley, 1981).
80. I.N. Mishustin, F. Myhrer and P.J. Siemens, Phys. Lett. 95B (1980) 361.
81. J.I. Kapusta and D. Strottman, Phys. Rev. C 23 (1981) 1282.
82. J.R. Wu, G.C. Chang and H.D. Holmgren, Phys. Rev. C 19 (1979) 659.
83. P.J. Siemens, private communication, 1981.
84. F. Hachenberg, H.C. Chiang and J. Hufner, Phys. Lett. 97B (1980) 183.
85. D.H. Boal and M. Soroushian, Preprint TRI-PP-81-7 (1981).
86. S.I.A. Garpman, S.K. Samaddar, D. Sperber and M. Zielinska-Pfabe, Phys. Lett. 92B (1980) 56.
87. C.Y. Wong, Symposium on Heavy Ion Physics from 10 to 200 MeV/nucleon, Brookhaven National Laboratory Report BNL-51115 (1979) p. 379.
88. H.H.K. Tang and C.Y. Wong, Phys. Rev. C 21 (1980) 1846.

† For clarity, many figures in this paper have been redrawn. References should be made to the authors of the originials for determination of precise numerical values.